Available online at www.sciencedirect.com
SCIENCE DIRECT®
Journal of Magnetic Resonance 173 (2005) 140–152
JMR Journal of Magnetic Resonance
www.elsevier.com/locate/jmr

Missing first points and phase artifact mutually entangled in FT NMR data—noniterative solution

Grzegorz Stoch[a,b,*], Zbigniew Olejniczak[b]

[a] Department of Physics, MRI Center, University of New Brunswick, P.O. Box 4400, Fredericton, Canada E3B 5A3
[b] The H. Niewodniczański Institute of Nuclear Physics, ul. Radzikowskiego 152, 31-342 Kraków, Poland

Received 5 December 2003; revised 21 July 2004
Available online 7 January 2005

Abstract

Even moderate distortion at the beginning of the NMR signal contributes significantly to the baseline in the reciprocal domain, when the FID-type experiment is considered. If constant phase artifact is also involved, the net problem cannot be resolved accurately, according to its constituents considered in separation. This issue is particularly severe for powder patterns in solids, featuring complex broadband spectra, which substantially mask the baseline behavior. The complete correction procedure should intrinsically deal with both artifacts, due to the mutual dependency. The aim of this work is to indicate the possibility for the exact treatment of baseline and constant phase artifacts together, providing precise measure whether the correction is successful. We have found the analytical, noniterative solution for this coupled problem in the closed form. In this paper, we introduce the correction efficiency concept in order to have the measure for the correction reliability of the resulting spectrum. Relevant efficiency parameter η is the subject for quantitative analysis resulting in certain constraints for the measurement. We have determined exemplar trends for this parameter as a function of experimental variables such as signal-to-noise ratio and missing points number. The method is model-free and drawn from the origin of the baseline artifact; therefore has potential to work for a broad range of applications.

Keywords: Model-free baseline correction; Phase correction; Variational principle; Band-limited signals; Free induction decay

1. Introduction

The real part of the experimental spectrum depicted in Fig. 1A represents our baseline problem [1]. Such a baseline is heavily distorted; its curvature is large and occupies that substantial part in the middle of the bandwidth where the spectral lines are present. Moreover, depicted spectrum is very broad, complex, and masks the actual behavior of the baseline in the relevant region. In such a case, the knowledge about the lineshape would be certainly useful for the baseline correction; unfortunately it is the task on its own and mostly the actual result of the subsequent analysis. Elementary requirement to study this complex lineshape, however, is to have the baseline already corrected. This mutual dependency in the spectral region makes it virtually impossible to deal with the lineshape analysis and the baseline correction both simultaneously and successfully. Corrected spectrum in Fig. 1B reveals its actual structure, which makes this issue easier to realize. This spectrum is the result of the correction method being the subject of this paper; in this point represents the desired target, which in comparison to Fig. 1A, makes the task and its difficulty established.

The following considerations apply to the correction issue of missing points and the constant phase present in NMR experiments, such as the Free Induction Decay, where the maximum of the signal builds up at the beginning of the timescale. The two artifacts are mutually

* Corresponding author. Fax: +1 506 453 4581.
E-mail address: stoch@unb.ca (G. Stoch).

1090-7807/$ - see front matter © 2005 Elsevier Inc. All rights reserved.
doi:10.1016/j.jmr.2004.11.025

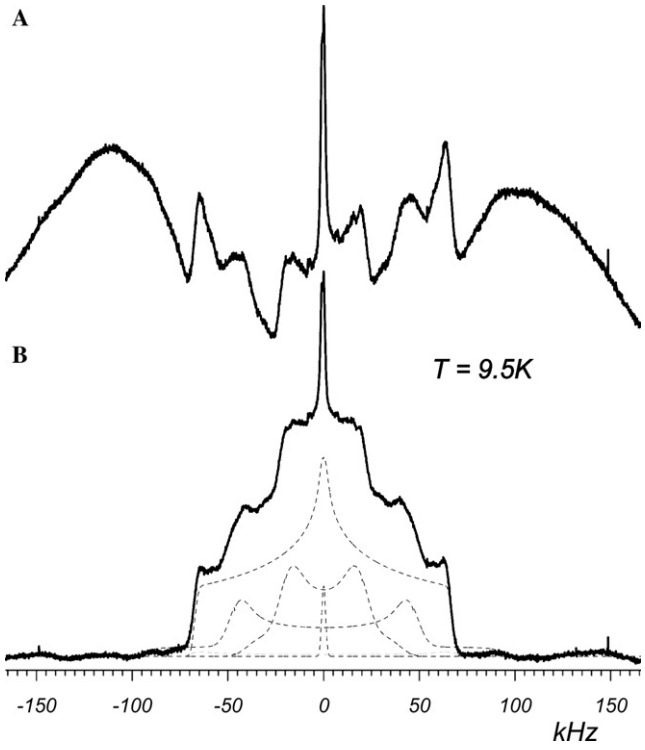

Fig. 1. (A) Experimental powder pattern as the result of missing four points in the time domain with constant phase artifact present. (B) The same data after successful correction using presented method. Correction enables both qualitative and quantitative analysis (B): several isotopomers in partially deuterated (30%) NH_4ClO_4 compound contribute to overall dynamics; relevant contributions (dashed lines) were obtained by fitting parameters of the process to the experimental data (solid line). Depicted only real parts of complex spectra, 2 μs dwell time [1].

dependent, and the net correction problem cannot be resolved accurately according to its constituents considered in separation. Ernst [2] noticed this difficulty very early in his work in 1968 devoted to phase correction. Since that time, the complex problem has not been resolved accurately for arbitrary number of points. Existing methods deal with the only one of the two artifacts at the time, usually assuming the other artifact is not present or corrected somehow. Zhu and Ad Bax in their papers [3–5] successfully analyze the problem for the phase and the only one point missing, using Linear Prediction method.

Because of the lineshape, which is a priori unknown, the model-dependent approach, such as Linear Prediction, cannot be used in this case. The simplest model-free method is the *running average*. It represents low-pass, finite-response, causal filter and is the particular instance of so-called Savitzky-Golayi smoothing filter [6]. When data has nonzero second derivative, such a filter reduces data value at the local maximum, depending on the local linewidth. If linewidths in the spectrum are narrower than the filter width, they can be removed by filtering. Pure and smooth baseline is obtained as the residue, which in turn might be subtracted from the actual spectrum making the problem resolved. In order for this approach to work, however, it must be both the filter width and the linewidths much narrower than the spectrum bandwidth. As it is clear both from Fig. 1 and the discussion, this is not our case, and such a method cannot be used either.

Let us summarize constitutive features for the method presented in this paper as well as the experimental motivation standing in the background.

(a) *Constant phase artifact*. We focus on the constant phase artifact, which is inevitable part of the experiment when the signal-to-noise ratio is small or usual phase cycling does not solve the problem. Fourier transformation of the signal is very sensitive to missing points coupled to even very small constant phase mismatch. This makes data interpretation difficult, especially for broad spectra such as in Fig. 1. Our approach assumes there do exist efficient methods for adjusting zero-time experimentally (as we know from practice) and this justifies neglecting of the linear phase artifact in the following considerations.

(b) *Arbitrary number of missing points*. To provide a sufficient bandwidth for broad spectra we need to set our dwell time sufficiently short. For the established *dead time*, as the result of hardware limitations, this constraint inevitably results in the increased missing points number, when the larger bandwidth is required. In the following, this number is considered as arbitrary, even though in our practice it does not exceed 10 points for complex spectrum (20 real unknowns).

(c) *Model-free approach*. Linear prediction implicitly assumes Lorentzian lineshape model (series of damped sinusoids in the time domain) and cannot be used successfully for arbitrary spectrum. In particular, it is obvious that for data in Fig. 1 (which is our prototypical case) this assumption is dramatically inadequate. The lineshape might also evolve with the temperature, which inclines towards a model-free approach further.

This preliminary consideration makes it clear that the strict formula describing artifact is needed, which would be formal starting point for the following correction method. Such an exact formula originates in properties of Discrete Fourier Transform and is presented below.

2. The dead time and DFT origin of the baseline

The NMR signal $f(t)$ from the probe is usually distorted at the beginning of the timescale $t = 0$. The reason for this is finite pulse width, probe ringing, and oscillating contribution from audio filters [7]. These is-

sues are intrinsic limitations for a spectrometer, making expected signal $s(t)$ distorted by $b(t)$ component. Function $b(t)$ is different from zero in the range $t \in [0, t_d]$ and identically zero otherwise (Fig. 2B). More detailed discussion on $b(t)$ origin and the physical nature of the distortion is not relevant to the following sections; it is enough to assume the t_d as short enough as compared to the total signal length.

However, even very short t_d, for example a few microseconds, might seriously influence analysis, as it is presented in Fig. 1. This local distortion $b(t)$ in the time domain is translated by Fourier transform into global, significantly varying function $B(\nu)$ in the frequency domain. Such a function is distributed over the entire bandwidth (Fig. 2A), which is the important difference as compared to local behavior of $b(t)$ in time (Fig. 2B). This function we call the *baseline*. According to the linearity of Fourier transformation, the distortion $B(\nu)$ is related to distorted and undistorted spectra in the same linear way as $b(t)$ to respective f and s signals:

$$s(t) = f(t) - b(t),$$

$$S(\nu) = F(\nu) - B(\nu). \tag{1}$$

Since $b(t)$ is rapidly quenched, and hence for $t > t_d$ is $b(t) \equiv 0$, the respective Fourier series is shortened to the number of complex components equal the number of missing points n_d:

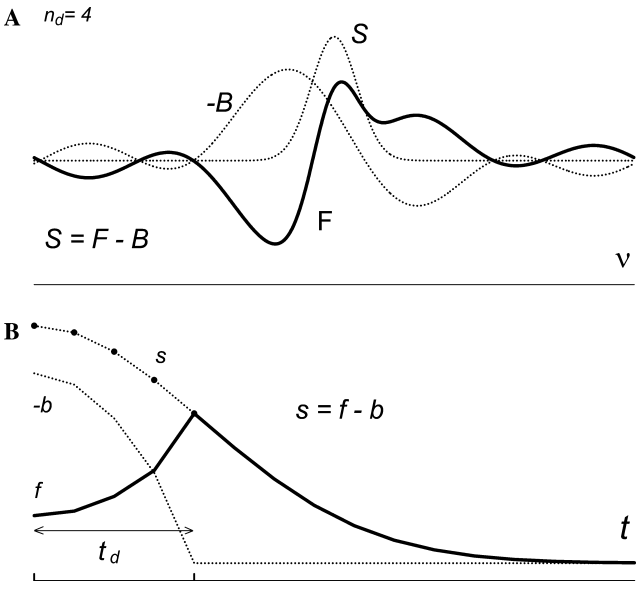

Fig. 2. (A) Distorted spectrum $F(\nu)$ as the sum of the background function $B(\nu)$ and undistorted spectrum $S(\nu)$: $F(\nu) = S(\nu) + B(\nu)$. (B) Similar relationship holds for the same data depicted in the time domain: distorted signal $f(t)$ is the sum of the background $b(t)$ and undistorted signal $s(t)$: $f(t) = s(t) + b(t)$. All relationships concern complex quantities, for simplicity only real parts are sketched. The number of distorted complex points within dead-time t_d is $n_d = 4$.

$$\begin{aligned} B(\nu) &= \sum_{k=0}^{N} b(t_k) \mathrm{e}^{-2\pi \mathrm{i} \nu k \Delta} \\ &= \sum_{k=0}^{n_d} b_k \mathrm{e}^{-2\pi \mathrm{i} \nu k \Delta} + \sum_{k=n_d+1}^{N} b_k \mathrm{e}^{-2\pi \mathrm{i} \nu k \Delta} \\ &= \sum_{k=0}^{n_d} b_k \mathrm{e}^{-2\pi \mathrm{i} \nu k \Delta}. \end{aligned} \tag{2}$$

Expression (2) is general and exact formula for the baseline $B(\nu)$ as the series of complex exponents, weighted by complex and unknown corrections to the signal b_k from the time domain. These unknowns are related through Eq. (1) to registered and expected signals within $[0, t_d]$ range. This type of distortion is the most pronounced for *FID*-based techniques, when the maximum of the signal concentrates close to $t = 0$. Spin-echo technique minimizes this effect; the signal starts far from the beginning of the timescale and distortion does not matter effectively.

In this paper, we assume the case in which the FID measurement is the best choice for experimental investigation, such as for solids with very short relaxation times T_2^*. In such a case finding undistorted values $s(t)$ within $[0, t_d]$ partition is vital for any subsequent analysis.

Values b_k in Eq. (2), representing corrections for registered signal samples f_k, are involved as unknowns for the correction process in the following considerations.

3. Existing correction schemes

A class of methods making use of Eq. (1) operates in the frequency domain, modeling the baseline $B(\nu)$ as some smooth function, preferably characterized by small parameter set $\{p_i\}$. That is, $B = B(\nu, p_i)$, similar to Bernstein polynomials in [8]. Baseline $B(\nu, p_i)$ can be fitted to the $F(\nu)$ spectrum with appropriate $\{p_i\}$ and subtracted according to Eq. (1) afterwards. These very direct approaches might be inadequate for broad lines (Fig. 1) where the region occupied by the spectrum is large and there is no base for any assumptions about $B(\nu, p_i)$ behavior. Most importantly, these approaches can at best be approximations for the generic form of the baseline in Eq. (2); therefore we reject them as secondary.

Another set of methods is characterized by their implicit or explicit assumption about the lineshape. Linear prediction by singular value decomposition (LPSVD) is the example [9–11] for the Lorentzian lineshape. Procedure is based on modeling data as the series of damped harmonics in the time domain. Each processed data point can be expressed as a weighted sum over some number of consecutive points. This leads to the construction of *data matrix* [10] and therefore to linear problem, being resolved with the SVD algorithm. The method works fine as long as data can be considered as Lorentzians in the frequency domain. As mentioned earlier, this constraint is

not acceptable for the case depicted in Fig. 1, which is frequent for powder patterns in solids.

There are also iterative approaches based on maximum-entropy principle, like MEM [13–15]. The goal is to maximize certain functional there, according to constraints introduced by Fourier transformation and experimental noise. The solution is obtained iteratively, so the aspect of both convergence and the initial guess must be taken into account. It is also recommended to make the resolution enhancement prior to correction there, as well as to estimate first data points by other methods [12]. Hence, the method is not self-contained or firmly stable and therefore cannot work for us either.

Golotvin and Williams [16] proposed the procedure, which is the variation of the averaging scheme discussed earlier, and for the similar reason cannot be applied successfully to our data. Their approach works sufficiently well for narrow lines though.

For the method proposed in this paper, particularly important is the class of so-called model-free approaches. Heuer and Haeberlen published in 1989 the prototypical paper in this field [12], and we believe that it was, conceptually, the starting point for any model-free approach, including recent ones [17–19]. Their paper contains the pioneering idea to use the information from the outside of the spectral region (we call this *region* Ω) in order to formulate the criterion for the solution. For the real spectrum it is presumed that there are no spectral lines or their remainders present in this region. That allows for the formulation of the linear equation set for missing points in the time domain. Noise inclusion makes existing equations to hold only approximately; therefore the problem is solved in the least squares sense, preserving linear character of the task. In this original formulation the paper does not address the constant phase problem, as well as does not propose convincing criterion for the success or the failure for the method itself. Furthermore, the method (*BCF*, Baseline Cosine Fitting) works for symmetric spectra only; general solution requires also combinations of sin functions.

In this work, we use the concept of the principle minimum, where the aspect of the noise is naturally self-contained. This allows for direct formulation of the appropriate equations set without any idealization for the problem. Still holds the assumption due to the Ω region, where it is expected to have no spectral lines present. Furthermore, this approach is easily generalized for the case with the phase artifact included. We address also the correction efficiency issue, as a quite separate concept.

4. Correction efficiency parameter η

The problem of the correction efficiency (let us call it η) concerns any correction scheme and it is convenient to consider this measure as universal concept. Note, that in order to get the measure of correction reliability it is not sufficient to analyze the error of the solution as the result of the input perturbation (noise). There are shown relevant examples in this paper (have a look forward in Fig. 5) making it clear, that raw error does not represent the actual reliability for the correction process: the baseline is likely corrected and the relevant error is very small; lineshape, however, might be hopelessly distorted by our correction instead. Solution error cannot reflect this phenomenon, because the actual signal (as it is for model-free approach) is not present in the constitutive principle for the solution. The method based on the frequency regions Ω with no spectral lines present does not explicitly refer to the signal.

The issue of the solution reliability is frequently mentioned in other papers in the context of instability or method convergence. However, even for perfectly convergent methods as based on closed expressions [17,18] the problem of the line distortion after correction remains valid, since, as pointed out, its origin is located outside of the correction method. One of the aspects is the propagation of the noise-induced perturbation across the linear or quasi-linear equations system. Even more important is that raw error δb does not carry any information about the physical reliability. What it describes this is only how well the initial criterion is fulfilled, namely how well corrected data approximate zero in Ω regions. In these regions there is no representation of the signal.

Therefore we have to supply physically motivated definition for the correction efficiency η, combining explicitly the solution error with the signal.

We derive such an expression from the first premises, such as energy balance principle. The original energy E of the system in the experiment is disturbed within t_d time (Fig. 3) and can be expressed as:

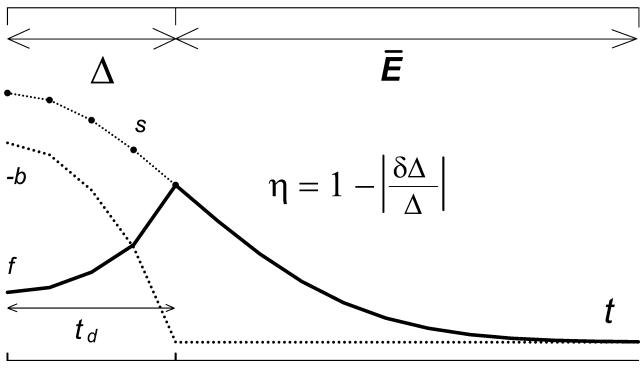

Fig. 3. True signal s within deadtime t_d is distorted and resulting signal f does not reflect original energy balance. Efficiency of the correction might be considered as the relationship between the energy Δ, attributed to the original undistorted points within time t_d, and the error $\delta\Delta$ dependent on the correction method.

$$E = \Delta + \overline{E}, \tag{3}$$

where

$$\Delta = \int_0^{t_d} |s(t)|^2 \, dt \quad \text{and} \quad \overline{E} = \int_{t_d}^{T} |s(t)|^2 \, dt = \int_{t_d}^{T} |f(t)|^2 \, dt. \tag{4}$$

By means of Δ parameter in Eq. (3) we ask *how much energy is missing as compared* to the true energy E. Quantity $\Delta = \Delta(b^m)$ depends on both b^m corrections and the signal f, due to Eqs. (1) and (4). It can be shown (see Appendix A) that above premises lead to the following definition for the correction efficiency:

$$\eta = 1 - \left| \frac{\delta\Delta}{\Delta} \right|. \tag{5}$$

Let us repeat that η is the measure for the physical reliability of the resulting spectrum. In the same time, $\delta\Delta(b^m)$ is related to the correction procedure error through b^m parameters directly. Both Δ and $\delta\Delta$ combine the solution error with the signal itself, fulfilling earlier postulate. Efficiency is independent of both total points number involved and the sampling rate. This is correct, as missing energy depends on the dead time value t_d in physical units. Extending the measurement time beyond the signal lifetime should not change the signal energy E significantly, except the noise contribution.

Furthermore, the same consideration (see Appendix A) leads to the conclusion about the legal range for the efficiency η. Providing we wish to stay with our estimation within one standard deviation confidence range, the relevant constraint for η is:

$$0 < \eta < 1. \tag{6}$$

Note that values less than zero, although formally available by means of Eq. (5), are explicitly excluded by Eq. (6). The same concerns the higher confidence level, for three standard deviations, where one obtains even more demanding requirement for the efficiency:

$$\frac{1}{3} < \eta < 1. \tag{7}$$

Thus, reasonable values for the efficiency parameter η vary form zero to 100%. Formulas for quantities Δ and $\delta\Delta$ originating in particular correction method, make it straightforward to determine η value.

5. The primary principle choice

To obtain desired corrections b^k we should supply some fundamental criterion for the method. In this section, we show the advantage of the particular choice, which will be our *primary principle* in the following considerations. Our choice is compared to the principle presented by Kuethe et al. [18,20] and we start with that one as first.

The *principle-minimum* can be arbitrarily chosen as to minimize the energy in the frequency region Ω where there are no spectral lines present:

$$\delta\left(I(b) = \int_\Omega \{S(\nu; b)\}^2 \, d\nu \right) = 0. \tag{8}$$

Note that Eq. (8) concerns *both* real and imaginary spectrum, and that Ω region choice is the intrinsic part of this principle. For a discrete case we have:

$$S_\nu = F_\nu - \sum_{n=0}^{n_d-1} b_n e_\nu^n, \quad \text{where } e_\nu^n = e^{-2\pi i n\nu/N} = (e^{n\nu})^* \quad \text{and} \quad n \in [0, n_d - 1]. \tag{9}$$

The summation goes over frequency region Ω in terms of the respective chain of indexes. Subsequent minimization over the real and imaginary parts for the baseline points b_m, leads to linear equations:

$$\sum_{m=0}^{n_d-1} b^m A_m^n = \sum_{\nu\in\Omega} F_\nu e^{n\nu}, \tag{10}$$

where $A_m^n = \sum_{\nu\in\Omega} e_{m\nu} e^{n\nu}$.

Spectrum F and chosen Ω partitioning in frequency are sufficient together to resolve above set of equations. The method originating in Eq. (8) yields corrected spectrum in Fig. 4C. That result shows obvious discrepancy as compared to original and undistorted simulation (Fig. 4A). For the Gaussian line, absorption mode vanishes rapidly as expected, what is not true for the dispersion data. This fact violates the initial assumption, concerning also the dispersion mode in Ω region, and produces the result that is far from true lineshape.

Instead of minimizing the norm of the spectrum, we can minimize the square of the real part only:

$$\delta\left(I(b) = \int_\Omega \{S^R(\nu; b)\}^2 \, d\nu \right) = 0. \tag{11}$$

Eq. (11) yields the linear equations system for the baseline points (for details, see Appendix A) independent of the imaginary part F^I:

$$\sum_{m=0}^{2n_d-1} x^m A_m^n = \sum_{\nu\in\Omega} F_\nu^R \alpha^{n\nu}, \tag{12}$$

where F^R is real spectrum taken in Ω frequency regions, defined earlier. Variables x^m are real numbers, representing real and imaginary parts of the baseline, aligned alternately as one vector ($2n_d$ real components) for n_d missing points. Constants A_m^n and $\alpha^{\nu n}$ depend on harmanic functions:

$$A_m^n = \sum_{\nu\in\Omega} \alpha^{\nu n} \alpha_{\nu m},$$

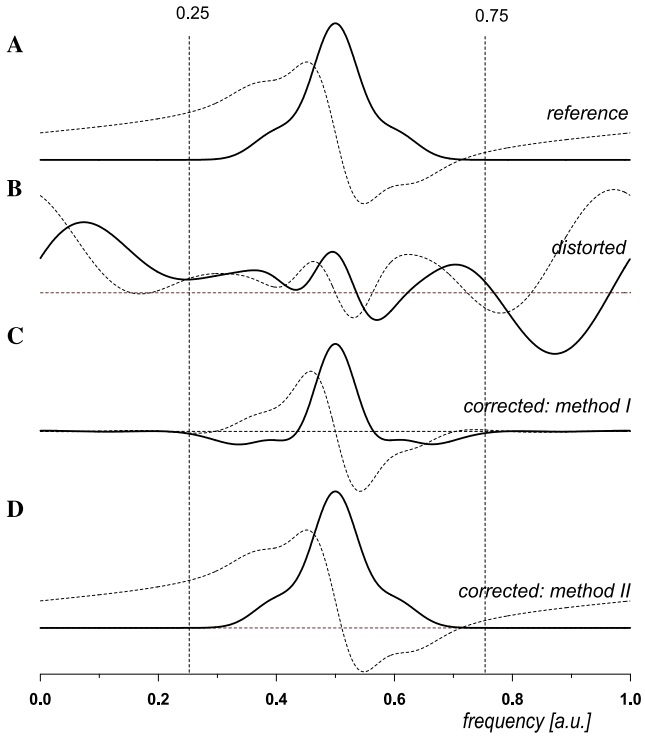

Fig. 4. Simulated noiseless spectra show the sensitivity to the principal criterion choice. Depicted both real and imaginary parts (solid and dashed lines, respectively). (A) Phase-sensitive reference spectrum. (B) First four complex points missing in the reference FID and the resulting distorted spectrum, (C) Distortion corrected by method I, (D) Distortion corrected by method II. Both methods minimize different functional in selected spectral regions. Method II results in remarkable agreement with the reference spectrum (A). The exemplar subspace Ω consists of two partitions: $\Omega = [0,0.25] \cup [0.75,1]$.

$$\alpha_{nv} = \begin{cases} n \text{ is even}: \cos\phi \\ \text{otherwise}: \sin\phi \end{cases}; \phi = 2\pi v \frac{n \gg 1}{N}; N - \text{total data number}.$$

Operation ($n \gg 1$) stands for integer division by 2.

Note, that despite primary principle concerns only real spectrum, both real and imaginary parts of missing points can be determined by means of Eq. (12) in the time domain.

The resulting correction (Fig. 4D) is successful, because the particular principle expressed in Eq. (11) is not violated this time, as it is the case for the same spectrum and Eq. (8).

We conclude that for broad lines and phase sensitive spectrum, criterion based solely on the absorption data (Fig. 4D) is advantageous over norm minimization (Fig. 4C). Both make use of the information taken from the outside of the spectral region. The first one takes only real part of the spectrum to calculate both real and imaginary parts of the baseline, while the norm approach includes also imaginary data for this purpose. In practice, it is nearly impossible to satisfy this version of the primary principle that requires imaginary spectrum to be close to zero within chosen regions Ω. The correction along the complex norm makes imaginary

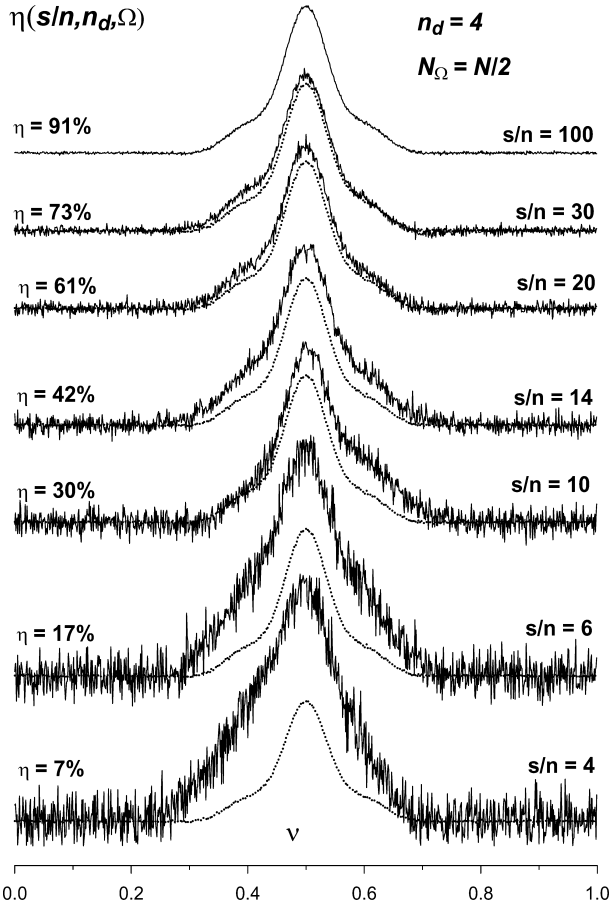

Fig. 5. Parameter η decreases due to signal to noise ratio decrease. The dashed line denotes the undistorted spectrum. The same synthetic spectrum, distortion and Ω subspace as in Fig. 4. Both visual inspection and numerical values confirm the usefulness of the parameter η as the measure for the correction efficiency.

data artificially minimized in those regions, which in turn makes the real part incorrect as well. The method considered in this paper is far more successful in this point (Fig. 4D), because its primary principle concerns more liberal assumptions due to imaginary spectrum.

6. Correction efficiency analysis

The solution of the linear system always exists if $\det(A) \neq 0$ in Eq. (12). Moreover, matrix A is independent of the experimental spectrum F, therefore it guarantees that the problem is *always* well-posed, without any computational singularities. In the following we discuss the error introduced solely by the experimental data and how it is reflected by correction efficiency η.

By means of Eq. (12) we can find quantities $\Delta(b^m)$, $\delta\Delta(b^m)$ relevant for the parameter η (see Appendix A). Efficiency η is general measure for the baseline correction with respect to some experimental variables:

$$\eta = \eta(\sigma_f, n_d, \Omega). \quad (13)$$

At the moment we do not see the way how to perform symbolic analysis of the function in Eq. (13) due to deep embroilment of $\{\sigma_f, n_d, \Omega\}$ variables in the solution. Nevertheless, its character can be examined numerically. This in turn, makes the analysis exemplar by nature, however, we may expect that obtained trends still hold in general.

6.1. Correction efficiency dependence on s/n

Simulated data depicted on Fig. 5 illustrate the change in the efficiency parameter η according to signal to noise ratio decrease. Correction procedure was performed each time for the same spectral lineshape, modified with different amount of the noise admixture. Each time the same four points were distorted in the time domain, resulting in similar distortion in frequency, to keep all aspects of this simulation repetitive, except for the noise level. This process was repeated for s/n ratio, ranging from 4 to 100. Results depicted in Fig. 5 shows that efficiency η decreases according to signal to noise ratio decrease. It is not surprising result, nevertheless this is the indication that parameter η is a good representation for the correction measure. Visual inspection stays in agreement with numerical values as the indepentent confirmation. The result formulates the requirement for sufficient s/n level in the experiment, to have subsequent correction successfully accomplished.

We have obtained efficiency η as the function of signal-to-noise ratio (s/n) for several values of missing points number (Fig. 6). It is interesting that function η has visible plateau starting from certain value of s/n ratio. It makes clear that there is no much sense to increase s/n ratio over certain limit, since it does not make any improvement for the correction. As it is seen form Fig. 6, for missing points number $n_d = 2$ this limit is s/n = 20 and for $n_d = 4$ this is s/n = 400. Since we know the dead time in our spectrometer, the guidelines for estimation *which level of the signal-to-noise ratio is suitable for us*, might be useful. We remember, however, that η is a function of several variables, which all matter in this calculation.

6.2. Correction efficiency dependence on Ω region

The choice for the Ω region, where there are no spectral lines present, is the intrinsic part of the method. In particular, what matters for the correction efficiency η, is *total length* of this region. Simulation in Fig. 7 was performed as a function of decreasing Ω region length, each time for the same spectral lineshape, number of missing points and the same noise level. It shows that efficiency parameter is very sensitive to the length of the Ω region, and decreases substantially when that length is decreased. In this point we draw the conclusion for the

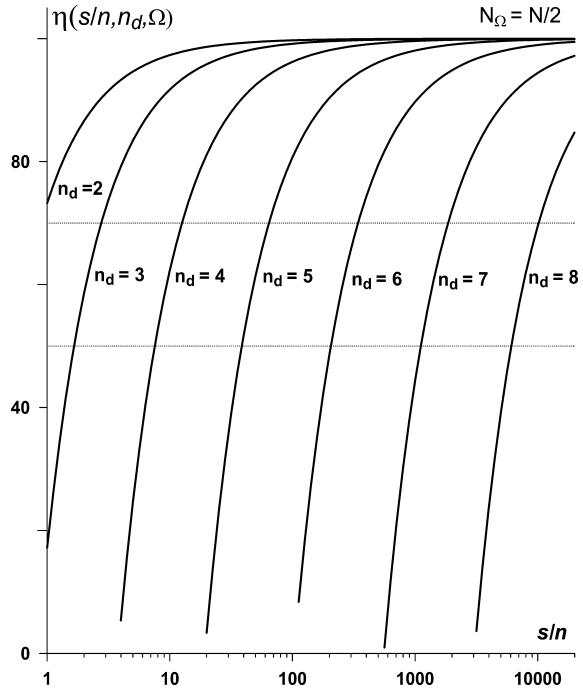

Fig. 6. Efficiency parameter η is the function dependent on signal to noise ratio. The necessity for signal to noise improvement is limited by certain s/n value, dependent on the missing points number in the measurement. Since the dead time in the spectrometer is known, the above trend is the guideline for estimation *which level of the signal to noise ratio is suitable for particular measurement*.

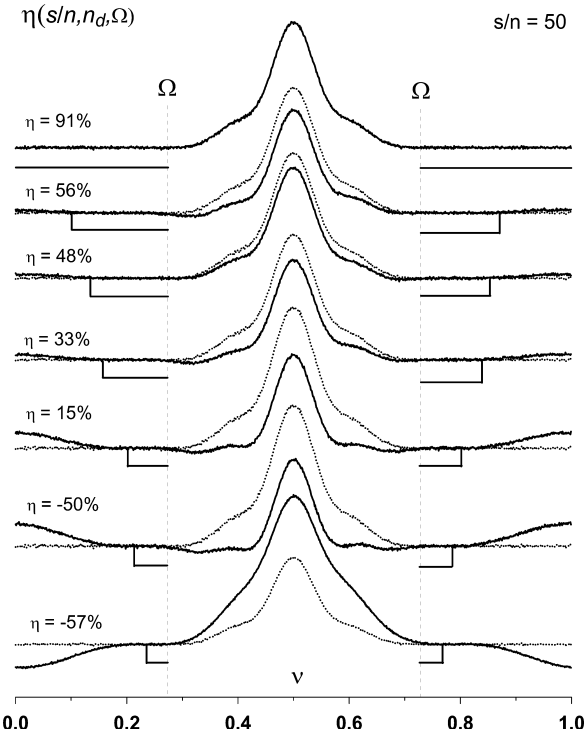

Fig. 7. Baseline correction efficiency η is dependent on the chosen Ω region length, depicted by rectangles. In the measurement, in order for subsequent correction to work, we need to set appropriate dwell time, making the Ω region large enough in frequency domain.

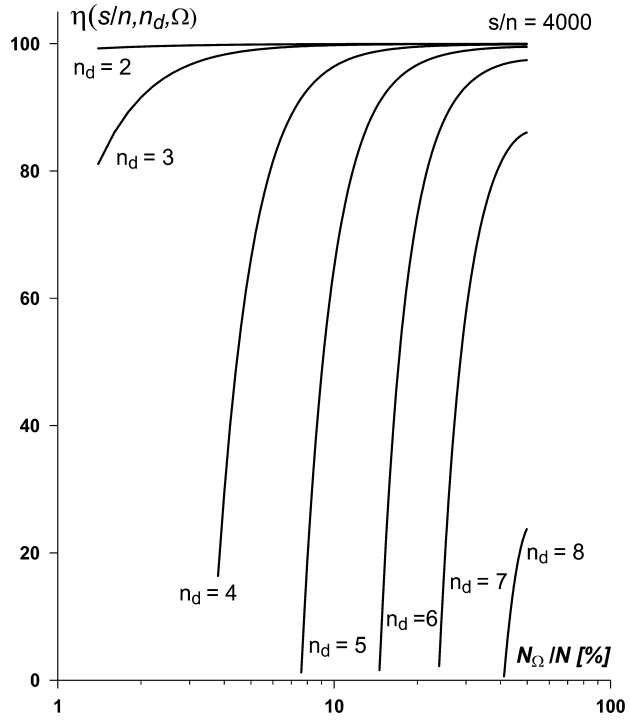

Fig. 8. The increase of the relative Ω length results in rapid correction efficiency increase. The trend is shown for several values of missing points n_d. The result makes it visible the similar plateau as for the dependence on the noise level. There is no significant efficiency improvement above the limit existing for the given number of missing points n_d.

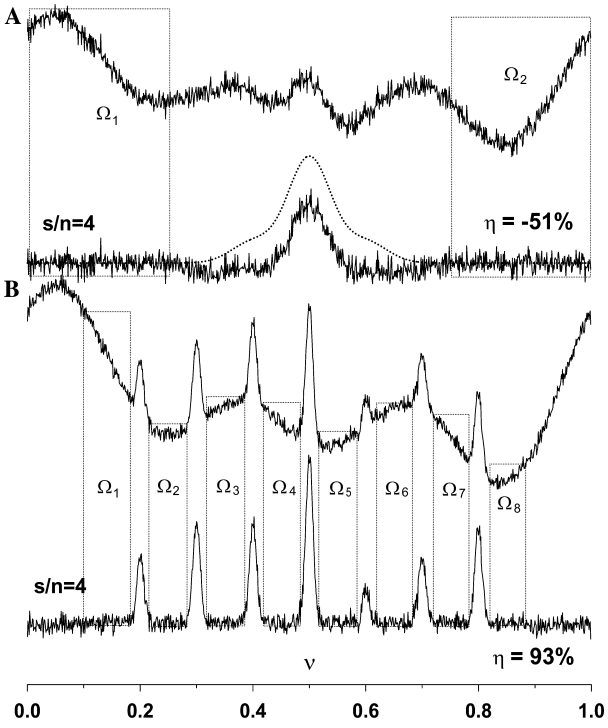

Fig. 9. Correction efficiency as a function of the Ω region distribution. It is much better efficiency ($\eta = 93\%$) whenever we deal with well-defined peaks uniformly distributed across the spectrum (B). In the case of powder pattern in solids (A), correction fails (compare the dashed line) and efficiency parameter η stays outside of any confidence range ($\eta < 0$). This is despite the same s/n ratio in both cases and the same Ω region length.

measurement, that the Ω region has to be a sufficiently large portion of our spectral band. Otherwise we might have problems with our correction, as it is depicted in Fig. 7. This issue (Fig. 1) determines mostly the upper limit for the dwell time for powder patterns in solids. Dependence on the relative baseline length is depicted in Fig. 8 for several missing points numbers. Relative length is the number of data points N_Ω in Ω region, related to the overall number of points N. There is clearly visible the upper limit for the baseline length, conditioning correction efficiency for the particular number of missing points. There is expected no significant efficiency improvement above this limit.

Region Ω, besides for the length, is characterized by its distribution. For the spectrum used consistently in all simulations in this paper, this distribution is obviously not uniform: there are two regions located on both extremes of the frequency band (Fig. 9A), as it is frequent for powder pattern in solids. We have compared this case to the simulation depicted in Fig. 9B, which stands for the measurement on the crystalline and oriented sample. Due to peak resolution, and therefore more uniform distribution of the baseline across the bandwidth, also larger efficiency η is obtained, as compared to the powder pattern. This result makes reasonable to expect better efficiency whenever we deal with well-defined peaks, uniformly distributed along the spectrum, such as in liquids, polymers or crystal samples.

6.3. Baseline length, missing points number, and oversampling

Expected strong dependence for the correction efficiency on the missing points number is confirmed by simulation (Fig. 10). Distorted spectrum was prepared the same way as for previous investigations. The same spectrum was corrected as a function of missing points number with the efficiency parameter as the result for one point in the figure. We have obtained the efficiency dependence on the missing points number for several s/n ratios. For the established s/n ratio this is visible rapid efficiency decrease due to the increasing number of missing points. Also this dependence has its own plateau, which is moved towards larger n_d for larger s/n ratios. It means that high signal to noise ratio permits for larger number of missing points at the same correction efficiency.

We have compared the two inverse trends in the correction efficiency behavior: one connected to the baseline length, and this related to the missing points number (represented in Figs. 8 and 10, respectively). In the presence of the dead time these two trends are coupled: when we decrease dwell time, in order to

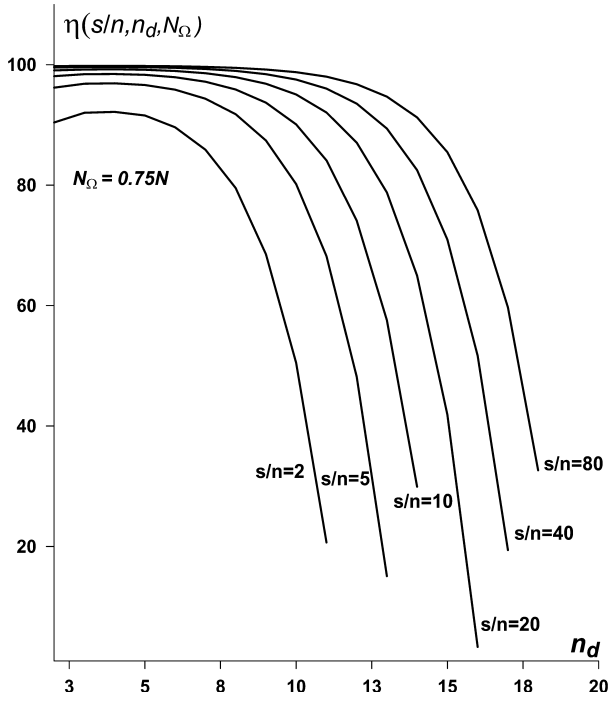

Fig. 10. Efficiency measure η as a function of n_{d} missing points number. There are depicted trends for several s/n ratios.

deliver sufficiently large Ω region in the frequency domain, the number of missing points increases accordingly. Magnitudes of these two inverse trends are comparable,

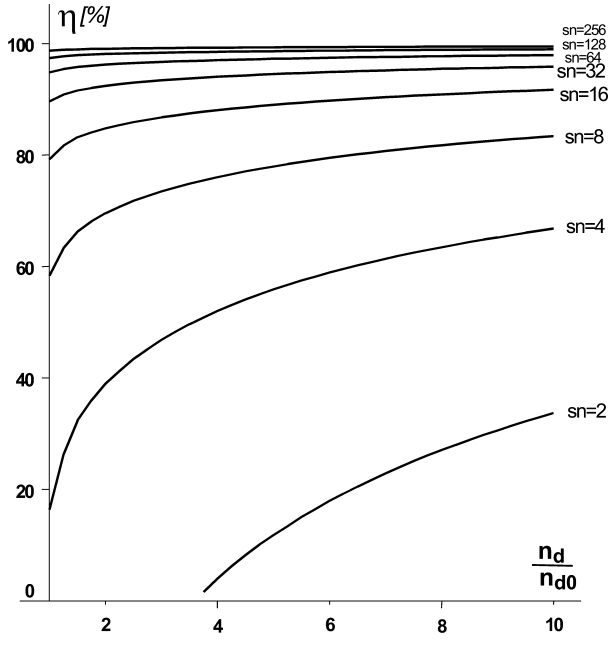

Fig. 11. When we decrease the dwell time in order to deliver sufficiently large Ω region for subsequent correction (according to Fig. 7), the number of missing points increases accordingly. The two inverse trends are coupled and depicted for several values of s/n ratio. n_0 is the number of missing points we start with in this simulation (common for all s/n). Trend shows that this is still advantageous to increase the bandwidth even by the expense of the missing points number increase.

therefore it is important for the measurement to settle, which one prevails in this coupling. From Fig. 11 it appears that bandwidth extension by oversampling is still advantageous in terms of the correction efficiency. It means, that correction performed for 400 missing points per 50,000 data would result in better spectrum than a similar correction for 4 and 500 data points. This result is *not evident* as based on visual inspection or just from simple reasoning. We conclude, that oversampling is still advantageous in the correction context.

7. Solution for missing points and constant phase

Our *general correction problem* is defined by the expression:

$$s(t) = \mathrm{e}^{\mathrm{i}\varphi} f(t) - b(t), \tag{14}$$

where φ is the phase distortion parameter and $b(t)$ is the baseline, both expected to be final results of the correction. Function $f(t)$ represents distorted signal, $s(t)$ the desired one. Primary principle given in Eq. (11) yields the following equation system:

$$\begin{cases} \sum_{m=0}^{2n_{\mathrm{d}}-1} x^m A_m^n = \sum_{\nu\in\Omega} W_\nu^{\mathrm{R}}(\tau)\alpha^{n\nu}, \\ p\tau^2 + q\tau - p = 0, \end{cases} \tag{15}$$

where $W_\nu(\varphi) = \mathrm{e}^{-\mathrm{i}\varphi}\cdot F_\nu$ and $\tau = \tan\varphi$. Other auxiliary substitutions are given by:

x_m, A_{mk}, and α_ν^m are defined in Eq.(12).

$$p = -\sum_{\mu\nu\in\Omega} g^{\mu\nu} F_\nu^{\mathrm{R}} F_\mu^{\mathrm{I}},$$

$$q = \sum_{\mu\nu\in\Omega} g^{\mu\nu} F_\nu^{\mathrm{R}} F_\mu^{\mathrm{R}} - \sum_{\mu\nu\in\Omega} g^{\mu\nu} F_\nu^{\mathrm{I}} F_\mu^{\mathrm{I}},$$

$$g_{\mu\nu} = \delta_{\mu\nu} - \sum_{m,n=0}^{2n_{\mathrm{d}}-1} (A^{-1})_{mn}\alpha_\mu^n \alpha_\nu^m.$$

The second equation in Eq. (15) is independent and can be resolved separately. The whole system in Eq. (15) can be thus explicitly resolved by elimination (see Appendix A) giving the solution for corrections x^m and phase φ:

$$\begin{cases} \varphi = \arctan(w \pm \sqrt{w^2-1}), \\ x^m = \frac{\sum_{\nu\in\Omega}\left[F_\nu^{\mathrm{R}}\cos\varphi - F_\nu^{\mathrm{I}}\sin\varphi\right]\sum_{k=0}^{2n_{\mathrm{d}}-1}\alpha^{k\nu}a_k^m}{\det(A)}, \end{cases} \tag{16}$$

where a_k^m is the algebraic complement to A_m^k and the auxiliary variable w is given by:

$$w = \frac{\sum_{\mu,\nu\in\Omega}\left(F_\nu^{\mathrm{R}}F_\mu^{\mathrm{R}} - F_\nu^{\mathrm{I}}F_\mu^{\mathrm{I}}\right)\sum_{n,m=0}^{2n_{\mathrm{d}}-1}\left[\delta^{\mu\nu} - (A)_{mn}^{-1}\alpha^{\mu n}\alpha^{\nu m}\right]}{2\sum_{\mu,\nu\in\Omega}F_\nu^{\mathrm{R}}F_\mu^{\mathrm{I}}\sum_{n,m=0}^{2n_{\mathrm{d}}-1}\left[\delta^{\mu\nu} - (A)_{mn}^{-1}\alpha^{\mu n}\alpha^{\nu m}\right]}.$$

One of the solutions in the square equation gives the maximum of the functional in Eq. (11) and should be rejected. It seems remarkable that the system in Eq. (15) is always well posed, since matrix A is symmetric, therefore always can be diagonalized.

8. Summary for the method

- The primary principle for the presented method is based on the assumption that system energy can be minimized separately for the real spectrum in certain Ω frequency regions. Such a choice makes the method immune to tails of the imaginary data.
- Variational principle directly yields the relevant equations, where the noise concept is naturally incorporated. Equations have no singularities, being all linear except for the phase, which the equation is quadratic one. Other approaches assume that the spectrum vanishes literally to zero in the selected Ω region, leading to an over-determinated linear equation system, which makes it difficult to analyse the relevant stability in terms of experimental variables.
- It can be shown (see Appendix A) that the problem is always well-posed for the presented formulation, without any singularities in the equation system. The actual reason for the correction failure might be the noise presence, in combination with the nature of the model-free approach. This issue is intrinsic and irremovable aspect for the problem.
- Simple nature of the equations makes it possible to obtain expressions for the correction efficiency η in the closed form. This quantity imposes constraints for experimental variables in the measurement.
- In this approach noise presence is explicitly irrelevant for the principle-minimum concept, although it is important issue when to consider correction efficiency η.

9. Conclusions

We have shown that the complex problem for both phase and baseline correction can be resolved in the closed form. Remarkable is noniterative character of the result. The final form of the solution in Eq. (16) is complicated, however expressed in terms of auxiliary variables becomes convenient for applications. The result does not depend on data model, is non-iterative and thus not sensitive to initial guess. The functional approach and its subsequent minimization (see also Appendix A) seems to be useful as a template for the following investigations. This in turn might benefit in further improvements in terms of criterion choice.

As it is discussed earlier, it is important to realize the distinction between simple error measure δb and the correction efficiency η. The first one contains no information about the corrected spectra, while the second is related both to the signal and the correction error. Efficiency parameter η is intended to be the measure for the physical reliability of the resulting spectrum after correction. Having this measure, it is also possible to optimize some experimental parameters prior to the measurement. In particular, we have shown that oversampling is advantageous in this context, even though the dimensionality of the problem increases.

Presented method makes use of that selected data, where it is presumed the absence of spectral lines in the real spectrum. This is only some part of the overall information available, and we consider this limitation as the drawback. This is the reason that Linear Prediction based schemes are expected to be more efficient, whenever experimental data follows Lorentzian lineshapes. We think that additional constraints found for this problem might be able to improve overall efficiency further.

Another drawback is poor computational efficiency for geometrical data-independent factor $g^{\mu\nu}$. The relevant calculation is based on many multiplications and trigonometric functions, which in terms of computational effort makes it similar to Fourier transformation without FFT scheme. On the other hand, since its data-independence, and assuming still the same Ω partitioning, $g^{\mu\nu}$ might be computed in advance and used many times.

Acknowledgments

One of us (G.S.) wish to thank *Professor Bruce J. Balcom* for his incentive to study the subject, discussion, and interesting remarks concerning MRI context of this work. Both authors express special thanks to *Michelle Dunphy* for reviewing the manuscript and discussion. The implementations of the algorithms described in the paper make use of FFTW source code ver. 2.1.3 by Matteo Frigo and Steven G. Johnson (*Massachusetts Institute of Technology*), which is efficient Fast Fourier Transform algorithm.

Appendix A

A.1. Notation

- R, I in expressions such as S^{R}, S^{I} denote the real and imaginary part, respectively.
- Notation such as a_n and a^n relates both symbols as follows: $a_n = (a^n)^*$, rising or lowering of the index makes the respective object conjugated.
- Einstein convention is applied, such as $a_t b^t = \sum_t a_t b^t$ and $A_\nu B^\nu = \sum_{\nu\in\Omega} A_\nu B^\nu$. *Latin* indexes ($a^k b_k$) concerns summation in the time domain which is always com-

pact and enumerates missing points, $k \in [0, 2n_d - 1]$ where n_d is missing points number. *Greek* indexes (such as in A_ν B^ν) concern the summation in the frequency domain within certain Ω space, which is not compact in general.

A.2. Distortion measure derivation

The original energy E of the system is disturbed in the experiment within t_d time and can be expressed as:

$$E = \Delta + \overline{E}, \tag{A.1}$$

where

$$\Delta = \int_0^{t_d} |s(t)|^2 \, dt,$$

$$\overline{E} = \int_{t_d}^{T} |s(t)|^2 \, dt = \int_{t_d}^{T} |f(t)|^2 \, dt. \tag{A.2}$$

We can define the energy ratio as the auxiliary variable χ:

$$\chi = \frac{\Delta}{E} = \frac{\Delta}{\overline{E} + \Delta} = \frac{\gamma}{\gamma + 1}, \quad \text{where } \gamma = \frac{\Delta}{\overline{E}}, \tag{A.3}$$

which is always bounded:

$$0 < \chi < 1. \tag{A.4}$$

The quantity gamma we call the *distortion* and we can obtain its relative error:

$$\frac{[\delta\gamma]^2}{\gamma^2} = \frac{[\delta\Delta]^2}{\Delta^2} + \frac{[\delta\overline{E}]^2}{\overline{E}^2}. \tag{A.5}$$

Calculation for $\overline{E}$ and Δ yields:

$$[\delta\overline{E}]^2 = 4\sigma_t^2 \overline{E},$$

$$[\delta\Delta]^2 = 4\sigma_t^2 s_m s^m + 4 \sum_{n=0}^{n_d - 1} \left\{ \left[s_n^R\right]^2 \left[\delta b_n^R\right]^2 + \left[s_n^I\right]^2 \left[\delta b_n^I\right]^2 \right\}, \tag{A.6}$$

which σ_t^2 is noise standard deviation in the time domain. Finally, we obtain distortion error:

$$\frac{[\delta\gamma]^2}{\gamma^2} = \frac{[\delta\Delta]^2}{\Delta^2} + \frac{4\sigma_t^2}{\overline{E}} \approx \frac{[\delta\Delta]^2}{\Delta^2}. \tag{A.7}$$

For increasing data points number N the contribution of the second component in (23) tends to zero. It is reasonable to connect this relative error of the distortion to the efficiency of the correction. Therefore we define the quantity:

$$\eta = 1 - \frac{\delta\gamma}{\gamma} = 1 - \left|\frac{\delta\Delta}{\Delta}\right| \tag{A.8}$$

and call it *correction efficiency*.

For the confidence level equal to one standard deviation, we have:

$$\chi + \delta\chi < 1. \tag{A.9}$$

Using definition for χ in Eq. (A.3) we have:

$$\frac{\delta\chi}{\chi} = (1 - \chi)\frac{\delta\gamma}{\gamma}. \tag{A.10}$$

Finally one obtains:

$$0 < \eta < 1. \tag{A.11}$$

In a similar way, it is possible to put more demanding requirements on the result, namely to postulate a higher confidence level (e.g., equal to three standard deviations). Then we have:

$$\frac{1}{3} < \eta < 1. \tag{A.12}$$

In conclusion, legal efficiency η values vary form zero to 100%.

A.2.1. Reduced solution

The expression for the absorption mode of the undistorted spectrum S is given by:

$$S_\nu^R(x) = F_\nu^R - \alpha_{m\nu} x^m. \tag{A.13}$$

Factor $\alpha_{m\nu}$ and corrections x^m are defined in Eq. (12). The minimization of $S_\nu^R S^{\nu R}$ requires:

$$\frac{\partial}{\partial x^m} S_\nu^R S^{\nu R} = 0 \tag{A.14}$$

and yields the linear equation set:

$$x^m \alpha^{\nu k} \alpha_{\nu m} = x^m A_m^k = F_\nu^R \alpha^{k\nu}, \tag{A.15}$$

where $A^{mk} = \alpha_\nu^m \alpha^{\nu k} = A^{km}$ is obviously symmetric and therefore can always be diagonalized. From $\alpha^{\nu k}$ definition it is that:

$$A_{1m} = A_{m1} = 0 \tag{A.16}$$

and each arbitrary value of x^1 satisfies Eq. (A.15). x^1 cannot be obtained by the intrinsic symmetry of the problem (this is the value of the imaginary spectrum integral). The true dimensionality for the system is $(2n_d - 1) \times (2n_d - 1)$. Instead of excluding the x^1 variable and the respective equation, we substitute $A^{11} = 1$ which removes this apparent singularity. The condition in Eq. (A.14) gives a so-called stationary point which is not automatically a minimum of $S_\nu^R S^{\nu R}$. Analysis of the matrix A^{nk} which is the second derivative of $S_\nu^R S^{\nu R}$ seems a cumbersome task, since the elements are the sums of harmonics and at the moment it is not clear how to handle them to prove the condition $d^2 S_\nu^R S^{\nu R} > 0$ formally. Instead, we may notice that values of $S_\nu^R S^{\nu R}$ are obviously bounded:

$$0 \leqslant S_\nu^R S^{\nu R}(x^m) < +\infty. \tag{A.17}$$

Value x^0 is responsible for the S^{R} offset and we can make it arbitrarily large ($x^0 \to \pm\infty$) as well as $|S^{\mathrm{R}}|$-hence upper bound. Derivatives of higher order than 2 (and equal to zero) are independent of $\{x^m\}$. The condition in Eq. (A.15) indicates that only one extremum point exists. Hence, keeping in mind the property in Eq. (A.17) and the fact that there are no higher order stationary points, we conclude that the condition in Eq. (A.15) determines the minimum of $S_v^{\mathrm{R}} S^{vR}$.

A.2.2. Standard deviation for reduced solution

Having the solution in Eq. (A.15) expressed as:

$$x^m = (A^{-1})_n^m F_v^{\mathrm{R}} \alpha^{nv} \tag{A.18}$$

and having that $x^m = x^m(F^{\mathrm{R}})$ is the function of data, we get the standard deviation $[\delta x^m]^2$:

$$[\delta x^m]^2 = \left|\frac{\partial x^m}{\partial F_v^{\mathrm{R}}}\right|^2 \left[\delta F_v^{\mathrm{R}}\right]^2 = \sigma_f^2 \sum_v [C^{mv}]^2, \tag{A.19}$$

where $C^{mv} = (A^{-1})_n^m \alpha^{nv}$ and $\sigma_f = \delta F$ is the noise variance and finally:

$$[\delta x^m]^2 = \sigma_f^2 [C^m]^2, \tag{A.20}$$

where $[C^m]^2 = \sum_v [C^{mv}]^2$.

This deviation is noise-dependent and could measure the error of the correction x^m. Since x^m is linearly dependent on F in Eq. (A.18), the derived expression in Eq. (A.19) holds also for larger σ_f values.

A.2.3. General solution

The problem for the signal with the phase artifact and missing points is represented by the equation:

$$S_v(x) = \mathrm{e}^{-\mathrm{i}\varphi} F_v - \alpha_{mv} x^m = W_v(\varphi) - \alpha_{mv} x^m, \tag{A.21}$$

where $W_v(\varphi) = \mathrm{e}^{-\mathrm{i}\varphi} \cdot F_v$. Minimization of $S_v^{\mathrm{R}} S^{vR}$ yields the linear equation set:

$$x^m A_m^n = W_v^{\mathrm{R}}(\varphi) \alpha^{nv} \tag{A.22}$$

due to derivation over x^m. The remaining derivation over φ leads to:

$$-(W_v^{\mathrm{R}} - x_n \alpha_v^n) W^{Iv} = 0. \tag{A.23}$$

Since the relationship: $x^m = (A^{-1})_k^m W_\mu^{\mathrm{R}} \alpha^{k\mu}$, Eq. (A.23) becomes:

$$-g_{\mu v} W^{\mathrm{R}\mu} W^{\mathrm{I}v} = 0, \tag{A.24}$$

where

$$g_{\mu v} = \delta_{\mu v} - (A^{-1})_{mn} \alpha_\mu^n \alpha_v^m \tag{A.25}$$

is data-independent symmetric tensor, $\delta_{\mu v}$ is the Kronecker symbol. Eq. (A.24) is the orthogonality relation in the frequency subspace, characterized by tensor $g = g(\Omega)$. In the absence of missing points ($g_{\mu v} = \delta_{\mu v}$) Eq. (A.24) solves pure phase correction problem. General issue results finally in the square equation for the unknown $\tau = \tan\varphi$:

$$p\tau^2 + q\tau - p = 0, \tag{A.26}$$

where

$$p = -g^{\mu v} F_v^{\mathrm{R}} F_\mu^{\mathrm{I}},$$

$$q = g^{\mu v} F_v^{\mathrm{R}} F_\mu^{\mathrm{R}} - g^{\mu v} F_v^{\mathrm{I}} F_\mu^{\mathrm{I}},$$

$$\Delta = q^2 + 4p^2. \tag{A.27}$$

It can be proven that quantity Δ is independent of φ. Due to $\Delta \geqslant 0$ the solution always exists. From Viete's formula it is seen that $\tau_1 \cdot \tau_2 = -1$, thus:

$$\varphi_1 = \varphi_2 - 90^\circ \tag{A.28}$$

assuming that $\varphi_2 > \varphi_1$ and $\varphi \in (-90^\circ, +90^\circ)$ domain.

Finally, we end up with the linear equations set in Eq. (A.22) together with Eq. (A.26). Both form the complete system for desired corrections and phase $\{x^m, \varphi\}$:

$$\begin{cases} x^m A_m^n = W_v^{\mathrm{R}}(\varphi) \alpha^{nv}, \\ p\tau^2 + q\tau - p = 0. \end{cases} \tag{A.29}$$

Since the square equation is independent of x^m one can solve it separately and substitute the result $\varphi = \arctan(\tau)$ into $W^{\mathrm{R}}(\varphi)$. Then we solve the linear equation set, and this way system in Eq. (A.29) is resolved. Having the substitution $x^m = (A^{-1})_k^m W_\mu^{\mathrm{R}} \alpha^{k\mu}$ we may reduce the minimization of $S_v^{\mathrm{R}} S^{vR}$ to a one-dimensional problem, represented by the second equation in Eq. (A.29). Now can be determined the condition for the minimum:

$$d^2 S_v^{\mathrm{R}} S^{vR}(\tau) > 0. \tag{A.30}$$

Providing in Eq. (A.26) that $\tau_1 < \tau_2$, the first derivative $[G^2(\tau)]' = -p\tau^2 - q\tau + p$ changes sign from "−" to "+" in $\tau = \tau_1$, when $p < 0$, and in $\tau = \tau_2$ when $p > 0$. Finally we have:

$$\begin{cases} p < 0, \ \text{then} : \tau_1 = \min., \tau_2 = \max, \\ p > 0, \ \text{then} : \tau_1 = \max., \tau_2 = \min, \end{cases} \tag{A.31}$$

which is the condition for the minimum.

A.2.4. Standard deviation for general solution

From Eq. (A.22) it follows that $[\delta x^m]^2$ is expressed by:

$$[\delta x^m]^2 = \sum_v [C^{mv}]^2 \left[\delta S_v^{\mathrm{R}}\right]^2, \tag{A.32}$$

where C^{mv} is defined in Eq. (A.19). Finally, we get:

$$[\delta x^m]^2 = \sigma_f^2 [C^m]^2 + (\delta\varphi)^2 [D^m]^2, \tag{A.33}$$

where it is defined: $[D^m]^2 = \sum_v [C^{mv}]^2 [W_v^{\mathrm{I}}]^2$. The $[\delta x^m]^2$ is charged by additional error connected to the phase stan-

dard deviation $[\delta\varphi]^2$ Prior to get this error, compute $[\delta t]^2$ from expression in Eq. (A.26):

$$[\delta\tau]^2 = \frac{\tau^2}{\gamma^2+1}[\delta\gamma]^2, \tag{A.34}$$

where $\gamma = q/2p$ and:

$$[\delta\gamma]^2 = \frac{1}{p^2}\left\{\frac{1}{4}[\delta q]^2 + \gamma^2[\delta p]^2\right\}. \tag{A.35}$$

The $[\delta p]^2$ and $[\delta q]^2$ deviations can be derived from the definitions of p and q in Eq. (A.26). The differentiation goes over F^{I} and F^{R}, namely:

$$[\delta p]^2 = \sigma_f^2 \sum_v \left\{ \left|\frac{\partial p}{\partial F_v^{\mathrm{R}}}\right|^2 + \left|\frac{\partial p}{\partial F_v^{\mathrm{I}}}\right|^2 \right\}. \tag{A.36}$$

Since $g^{\mu\nu}$ is data-independent, after differentiation we get:

$$[\delta p]^2 = \sigma_f^2 \sum_v \left\{ \left(g^{\nu\mu}F_\mu^{\mathrm{R}}\right)^2 + \left(g^{\nu\mu}F_\mu^{\mathrm{I}}\right)^2 \right\}. \tag{A.37}$$

A similar calculation for $[\delta q]^2$ yields:

$$[\delta q]^2 = 4\cdot[\delta p]^2 \tag{A.38}$$

and finally $[\delta\gamma]^2 = \{1+\gamma^2\}[\delta p]^2/p^2$. Now we get the expression for $[\delta\tau]^2$:

$$[\delta\tau]^2 = \tau^2[\delta p/p]^2 \tag{A.39}$$

and hence for $[\delta\varphi]^2$:

$$[\delta\varphi]^2 = \frac{\tau^2}{(\tau^2+1)^2}\left[\frac{\delta p}{p}\right]^2 = \frac{[\delta p]^2}{\Delta} \tag{A.40}$$

and finally:

$$[\delta\varphi]^2 = \frac{\sigma_f^2}{\Delta}\sum_v \left\{ \left(g^{\nu\mu}F_\mu^{\mathrm{R}}\right)^2 + \left(g^{\nu\mu}F_\mu^{\mathrm{I}}\right)^2 \right\}. \tag{A.41}$$

Note that expression Eq. (A.41) is independent of φ. From that we get final expression for $[\delta x^m]^2$:

$$[\delta x^m]^2 = \sigma_f^2\left\{[C^m]^2 + \frac{[D^m]^2}{\Delta}\sum_v[(g^{\nu\mu}F_\mu^{\mathrm{R}})^2 + (g^{\nu\mu}F_\mu^{\mathrm{I}})^2]\right\}. \tag{A.42}$$

Since $[\delta\varphi]^2$ is entirely determined by the experimental data F and the Ω choice, the Eqs. (A.41) and (A.42) are sufficient to obtain the respective errors. Both of them do not depend on φ, despite of one square equation in the system Eq. (A.29).

References

[1] G. Stoch, A. Birczyński, Z.T. Lalowicz, Z. Olejniczak, A novel analysis method for complex ^{2}H NMR spectra as applied to partially deuterated $(NH_4)_2SnCl_6$, Mol. Phys. Rep. 33 (2001) 127.

[2] R.R. Ernst, Numerical Hilbert transform and automatic phase correction in magnetic resonance spectroscopy, J. Magn. Reson. 1 (1968) 7–26.

[3] Ad. Bax, M. Ikura, L.E. Kay, G. Zhu, Removal of F1 baseline distortion and optimization of folding in multi-dimensional NMR spectra, J. Magn. Reson. 91 (1991) 174–178.

[4] G. Zhu, Ad. Bax, Improved linear prediction of truncated damped sinusoids using modified backward–forward linear prediction, J. Magn. Reson. 100 (1992) 202–207.

[5] G. Zhu, D. Torchia, Ad. Bax, Discrete fourier transformation of NMR signals. the relationship between sampling delay time and spectral baseline, J. Magn. Reson. Series A 105 (1993) 219–222.

[6] W.H. Press, B.P. Flannery, S.A. Teukolsky, W.T. Vetterling, Numerical recipes, in: C: The Art of Scientific Computing, second ed., Cambridge University Press, New York, 1997, p. 650.

[7] C. Tang, An analysis of baseline distortion and offset in NMR spectra, J. Magn. Reson. 109 (1994) 232–240.

[8] D.E. Brown, Fully automated baseline correction of 1D and 2D NMR spectra using Bernstein polynomials, J. Magn. Reson. 114 (1995) 268–270.

[9] H. Barkhuijsen, R. de Beer, W.M.M.J. Boveè, D. van Ormondt, Retrieval of frequencies, amplitudes, damping factors, and phases from time-domain signals using a linear least-squares procedure, J. Magn. Reson. 61 (1985) 465–481.

[10] H. Barkhuijsen, R. de Beer, D. van Ormondt, Error theory for time-domain signal analysis with linear prediction and singular value decomposition, J. Magn. Reson. 67 (1986) 371–375.

[11] V.C. Klema, A.J. Laub, IEEE Trans. Autom. Control AC-25 (2) (1980) 164.

[12] A. Heuer, U. Haeberlen, A new method for suppressing baseline distortions in FT NMR, J. Magn. Reson. 85 (1989) 79–94.

[13] S.F. Gull, G.J. Daniell, Nature (London) 272 (1978) 686.

[14] D.S. Stephenson, in: J.W. Emsley, J. Feeney, L.H. Sutcliffe, (Eds.), Progress in NMR Spectroscopy, vol. 20, Pergamon, Oxford.

[15] E.D. Laue, K.O.B. Pollard, J. Skilling, J. Staunton, A.C. Sutkowski, Use of maximum entrophy method to correct for acoustic ringing and pulse breakthrough in ^{17}O NMR spectra, J. Magn. Reson. 72 (1987) 493–501.

[16] S. Golotvin, A. Williams, Improved baseline recognition and modeling of FT NMR spectra, J. Magn. Reson. 146 (2000) 122–125.

[17] D.P. Madio, H.M. Gach, I.J. Lowe, Ultra-fast velocity imaging in stenotically produced turbulent jets using RUFIS, Magn. Reson. Med. 39 (1988) 574–580.

[18] D.O. Kuethe, A. Caprihan, E. Fukushima, R.A. Waggoner, Imaging lungs using inert fluorinated gases, Magn. Reson. Med. 39 (1998) 85–88.

[19] S.K. Plevritis, A. Macovski, IEEE Trans. Med. Imaging 14 (1995) 487–497.

[20] D.O. Kuethe, A. Caprihan, I.J. Lowe, D.P. Madio, H.M. Gach, Transforming NMR data despite missing points, J. Magn. Reson. 139 (1999) 18–25.